ORIGINAL PAPER

Scaling Down the Great Egypt Pyramids to Enhance CO_2 Splitting in a Micro DBD Reactor

Deema Khunda[1,2] · Sirui Li[1,3] · Nikolay Cherkasov[1] · Alan Chaffee[2] ·
Evgeny V. Rebrov[1,3]

Abstract

The CO_2 splitting reaction has been investigated in a plate-to-plate micro DBD reactor with a high voltage electrode having pyramid charge injection points. The presence of sharp points (pyramids) creates zones with enhanced electric field around them. The minimum discharge voltage in the pyramid micro DBD reactor reduced from 6.5 to 5.2 kV (peak-to-peak). At the same time, the CO_2 conversion increased 1.5 times as compared to that in the reactor with a flat electrode. Lowering the discharge gap from 0.50 to 0.25 mm resulted in more intense microdischarges, further increasing CO_2 conversion by 1.3 times. At the same time, the energy efficiency increased further by 1.3 times. There exists an optimum residence time of 0.5 ms as a result of an interplay between plasma contact time and flow non-uniformity. The highest energy efficiency of 20% was obtained at a 3 W power, achieving a CO_2 conversion of 16%.

Introduction

Plasma technologies have garnered increasing interest as a renewable route for CO_2 gas processing to produce syngas and other intermediary products. Plasma-based solutions offer a system in which surplus electrical energy from renewable sources is used to convert CO_2 into value-added chemicals and fuels. They are compact, robust and flexible under various operating conditions such as temporal changes in inlet gas composition and input energy [1]. This is particularly useful when compared to other renewable gas processing routes such as bioreactors or CO_2 mineralisation which are operable under specific temperature and photolytic conditions [2]. Plasma technology's adaptability to fluctuations in input energy could enhance intensification of CO_2 processing systems

✉ Evgeny V. Rebrov
  e.rebrov@warwick.ac.uk; e.rebrov@tue.nl

1 School of Engineering, University of Warwick, Coventry, UK

2 School of Chemistry, Monash University, Melbourne, Victoria, Australia

3 Department of Chemical Engineering and Chemistry, Eindhoven University of Technology, Eindhoven, The Netherlands

[3]. Process intensification is of particular importance for CO_2 splitting reaction because it is highly endothermic [4]. Radiative heal loss increase with the fourth power of temperature, therefore energy-concentrated routes are more suitable than thermal decomposition [5].

Plasma can be classified into two broad types, thermal plasma, and non-thermal plasmas (NTP) [6]. While thermal plasma has been successfully adapted in industrial applications such as plasma arcs used in the destruction of hazardous chemicals, ozone generation, and enriching fuel with syngas in combustion engines, NTP has only been applied in small commercial projects for gas processing [7]. Despite the fact that carbon capture and storage (CCS) facilities provide around 40 million ton CO_2 storage capacity [8] therefore significant substrate of CO_2, NTP is not employed at industrial scale due to its low energy efficiency [5].

Pure CO_2 splitting in dielectric barrier discharge (DBD) reactors has been extensively studied, and energy efficiency above 60% was shown to be possible, resulting in a solar-to-CO or syngas conversion efficiency above 20% [6]. Several factors influencing conversion and energy efficiency (EE) were identified. The CO_2 conversion increases both with applied power and residence time inside the plasma zone [9, 10]. The residence time has a more pronounced effect than power, with longer residence times, higher conversion is achieved. However longer residence times require low gas flow rates and this limits scale up of plasma reactors to industrial scale. The CO_2 conversion can further be increased by addition of methane or H_2 as a co-reactant decreasing the reaction enthalpy [11–14], use of catalysts [15, 16], by cooling of the ground electrode [17], by specific electrode geometry, or by a combination of these factors. Over heterogeneous catalysts, the CO_2 adsorption increases at a higher catalyst basicity providing higher conversion [18]. In dry reforming of methane (DRM), a CO_2 conversion of 39% was reported over a Fe/SiO_2 catalyst [19] and 21.4% over metal oxides ($Ni/\gamma-Al_2O_3$, $Ag/\gamma-Al_2O_3$) [18]. Much higher CO_2 conversion was demonstrated in CO_2 hydrogenation as compared to DRM, reaching up to 70% over a 15 wt.% $Ni-CeO_2/Al_2O_3$ catalyst yet at a rather high temperature of at 150 °C [20].

Dielectric properties of the reactor material were shown to impact conversion in both tubular and planar DBD reactors [21, 22]. Zhang et al. found that the CO_2 conversion increased to 18% in a packed bed DBD reactor as the shorter distance between the glass particles enhanced the electric field [23]. Navascués et al. demonstrated that ferroelectric lead zirconate titanate (PZT) particles provided a CO_2 conversion of 10% and an energy efficiency of 11% in a plate-to-plate DBD reactor [24]. The influence of reactor geometry on CO_2 splitting in DBD reactors has been less extensively studied than the effect of operating parameters. In recent studies, the pin-to-electrode arrangement has garnered interest after promising results in glow discharge plasma mode with a 45% energy efficiency at a CO_2 conversion of 28% [25]. The pin to electrode configuration was previously studied by Lee et al. [26]. A more filamentary discharge was observed as opposed to the long streamer discharge in conventional DBD reactors [27, 28]. A multi-pin electrode DBD was compared to the plane electrode for NO_x removal [28]. It was shown that the multi-pin reactor operated at lower voltage and had higher conversion at the same input power.

The presence of sharp points (pyramids or protrusions) in the high voltage electrode creates zones with enhanced electric field around them [29, 30]. The pyramid electrode allows the reactor to operate at a lower applied voltage because the sharp points of the pyramid structure distort and rotate the electric field around the tip [31]. The gradient of electric field around the sharp point can create electrodynamic flow of the gas resulting in a more uniform plasma [30]. The advantage offered by novel electrode surface designs has scarcely been investigated for CO_2 utilization, some authors investigated single point

electrode and ring for CO_2 reforming with methane [24] and others investigated pyramid electrode surface for NO removal [32].

In our previous study, a sharp maximum in CO_2 conversion was observed at a gas temperature of 90 °C [17]. Such temperature dependence was explained by two competing phenomena: increasing the rate of CO_2 dissociation via the vibrational ladder climbing process at lower temperatures which competes with a decrease of the reaction rate via the Arrhenius law. In this study, a charge injector DBD was fabricated by engraving pyramid-shaped micro tips on the high voltage (HV) electrode. The sharp edges of these tips increase the rate of secondary electron and field emission, leading to higher density of rotational and vibrational states of CO_2 molecules. The excited CO_2 molecules can easily dissociate at normal temperature and pressure. The sharp tips or edges concentrate the electric field [29], leading to a high surface charge density and enhancing the probability of vibrational excitation or ionization of CO_2 molecules. The charge density is inversely proportional to the area of curvature of the surface [33]. Thus, sharp edges with small curvature have higher charge density, resulting in a stronger electric field at the tip where the density of electrons is much larger. It is still rather expensive to fabricate electrodes with very sharp tips. Therefore, when designing the structure, the tip curvature was limited to 25 µm.

To evaluate the benefits of micro DBD reactors, we compared the conversion and energy efficiency in the pyramid electrode DBD with a conventional flat electrode DBD reactor. Some of the most important design parameters are the size of the gap in which plasma forms and the distance along the length in the flow direction for which the two electrodes overlap. These determine the volume of the plasma region and control the contact time of CO_2 molecules with the plasma. Additional parameters include the geometric shape of the electrodes themselves and the temperature of the ground electrode as it majorly determines the gas temperature in the discharge gap. The effect of discharge gap size, residence time and ground electrode temperature on CO_2 conversion and energy efficiency was studied.

Experimental

The ground electrode constituted of a brass plate with a diameter of 19.5 mm and was engraved with a cooling channel to maintained the desired temperature with a coolant flow. Two high voltage (HV) electrodes were used in this study. The flat HV electrode was made of a titanuim disk of 23 mm diameter (Fig. 1a). The pyramid HV electrode (also made of titanim disk) with 160 pyramids was fabricated by ANFF-SA, University of South Australia (Fig. 1b). The dimensions of pyramides are shown in Figs. 1c and 1d. The pyramids have a base of 1×1 mm and a hight of 1 mm. Such shape of pyramids allows a threefold electric field enhancement above the top pyramid plane where the gap distance is 0.5 mm.

The pyramids were positioned at a pitch of 1.5 mm in both directions. There are no infinitely sharp points that exist in reality, and the curvature radius of the tip was 25 µm. To avoid the arcing in between the edge of the HV electrode and the ground electrode, the ground electrode was covered with a 200 µm nonporous dielectric mica layer. Both electrodes were enclosed in a cylindrical quartz window with a sealed peripheral region. The gas entered the plasma zone through a small slit of 0.3 mm between the edge of mica film and the quartz window. The gas is withdrawn from the opposite side of the electrode. The window allowed optical studies performed during plasma experiments.
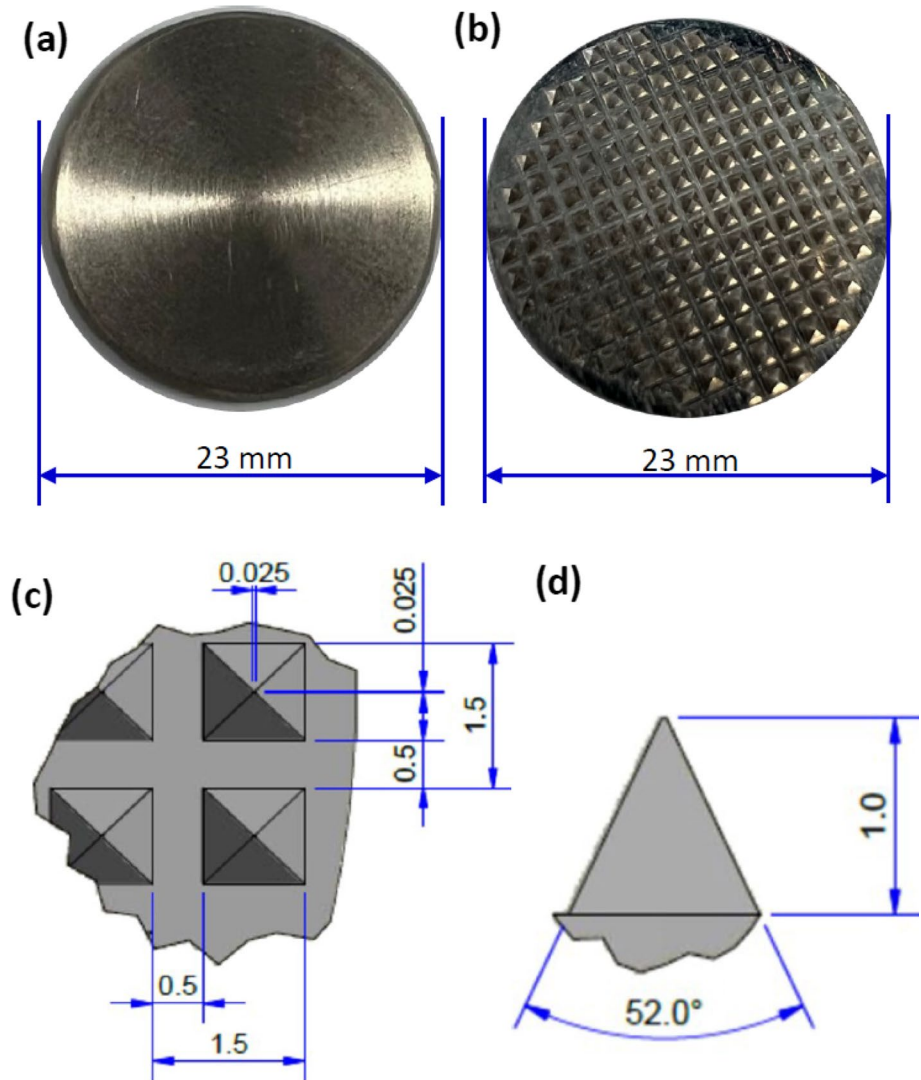
Fig. 1 A photograph of **a** flat electrode and **b** pyramid array electrode. **c** Top and **d** side view of pyramids and their dimensions

Two identical plate-to-plate reactors, the pyramid electrode microDBD, and flat electrode micro DBD were used in the experiments (Fig. 2).

The bottom electrode was grounded and the upper electrode was connected to a high voltage power supply (G2000, Redline Technologies). The gap distance between the electrodes was fixed with an adjustable screw located at the top of the HV electrode. In the flat electrode DBD, the gap is the distance between the surface of HV electrode and the dielectric film. In the pyramid electrode DBD, the gap is the distance between the pyramid top plane and the dielectric film. The high-voltage waveforms, cause plasma to form by ionizing CO_2 gas that flows between the two electrodes. A Rogowski coil (type 6600, Pearson) and a high voltage probe

Fig. 2 Schematic view of the microelecrode DBD plasma reactor
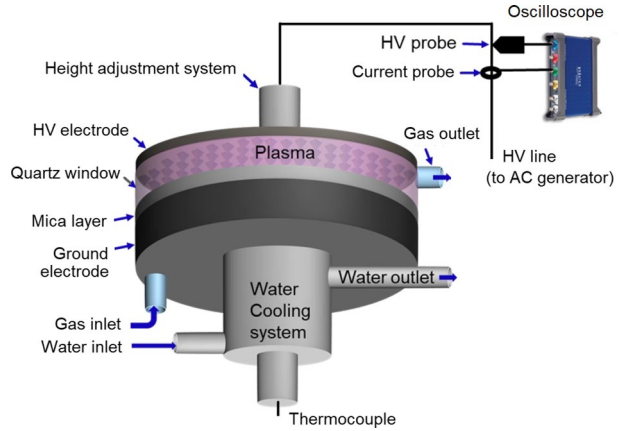
(P6015A 1000X, Tektronix) were employed to measure current and voltage, respectively, and the signals were captured using an oscilloscope (3000 series, Picoscope). The data were averaged over 13 cycles. A capacitor was introduced to the ground line for monitoring the electric charges generated in the plasma. Adding the capacitor creates a Thévenin-equivalent electrical circuit which integrates the total charge over the time of the discharge. The capacitance value of this capacitor is usually a factor of about 40–100 greater than the effective capacitance of the DBD reactor and plasma ($C_{cell} = 10$ nF, capacitor, $C_a = 400$ nF in this study). The effective reactor capacitance (C_{cell}) was calculated from the dielectric layer capacitance (C_d) and the gas capacitance (C_g):

$$\frac{1}{C_{cell}} = \frac{1}{C_d} + \frac{1}{C_g} \tag{1}$$

The breakdown voltage was detected by the oscilloscope and recorded for each electrode as a function of the electrode temperature. The CO_2 gas was cooled to the desired temperature (263–293 K) in a heat-exchanger (Lauda) and fed to the reactor with a MFC (Bronkhorst). The temperature of the outlet flow and the ground electrode was measured with thermcouples. The voltage and current signals were plotted to generate a Lissajous figure. The area of this figure was used to calculate the mean power dissipation during gas discharge [34, 35], where the power dissipated in one cycle is calculated by Eq. 2 [36, 37].

$$P = f \int_0^T V(t)I(t)dt \tag{2}$$

where f is the frequency, V is the voltage, and I is the current. When we refer to power consumption, we specifically mean the power dissipated in the plasma itself rather than the total amount of electrical power drawn by the system from the wall.

The product mixture was analyzed by a GC (Shimadu 2010) equipped with a flame ionization and thermal conductivity detectors. N_2 was used as an external standard. The CO_2 conversion was calculated by Eq. 3.

$$X_{CO_2}(\%) = \frac{\dot{n}_{CO_2,i} - \dot{n}_{CO_2,o}}{\dot{n}_{CO_2,i}} \times 100, \tag{3}$$

where $\dot{n}_{CO_2,i}$ and $\dot{n}_{CO_2,o}$ are inlet and outlet molar flow rate of CO_2 gas. Due to the volume expansion in the course of the reaction, the molar flow rates were used instead of concentration [38].

The energy efficiency η was calculated by Eq. 4.

$$\eta(\%) = \frac{X_{CO2} \times F_V \times \Delta H^o_{298}}{P \times V_m} \tag{4}$$

where ΔH^o_{298} is the standard reaction enthalpy of CO_2 splitting reaction, V_m is the gas molar volume (22.4 $Lmol^{-1}$).

## Results and Discussion

Discharge Analysis

In order to find out the operational window for stable plasma discharges, the breakdown voltage was evaluated in the micro DBD reactors with the flat and pyramid electrodes at different temperatures (Fig. 3a). For the flat electrode, the breakdown occurs at 6.5 and 7.0 kV peak-to-peak at 293 and 273 K, respectively. When the temperature decreases, the gas density increases, and the electron mean free path becomes shorter. The energy of electron is proportional to the product of the intensity of electric filed and the mean free path [39]. Therefore, the electrons gain less energy before the collision with other species reducing the probability of gas breakdown at lower temperatures. This trend agrees with previous studies [40]. However, for the pyramid electrode, the minimum voltage was considerably lower (5.2 kV peak-to-peak) at all temperatures studied. The intense electric field around the tip causes gas breakdown at a lower applied voltage than flat. Once the sharp tip initiates breakdown, the electric field accelerates the liberated electrons. A chain reaction will begin leading to avalanche breakdown, enabling the low voltage to maintain plasma operation.

The reactor with flat electrode has a considerably higher power consumption (Fig. 3b) which further increased as the temperature decreased from 293 to 263 K. The difference in power consumption at 263 K was 3 times higher than in the reactor with pyramid electrode.

The QV plot (Lissajous figure) shows the behaviour of the two reactors as the voltage increases from 6.0 to 8.5 kV (Fig. 4). The Lissajous figure is closed as the net charge transported in a single cycle is zero. The area of the closed loop gives the mean energy dissipation (power) in plasma. At a voltage of 6.0 kV peak-to-peak, the smaller charge dissipation occurs over the pyramid electrode which is due to the smaller current peaks in the flat electrode at the same applied voltage. Due to the ease of charge injection, pyramid electrodes exhibit a higher peak discharge current compared to flat electrodes. This can also be seen in Fig. 5 as higher current produces more visible light near the tips of pyramids.

The visual character of the plasma discharge is an indicator of the performance of the plasma reactor. Specifically, there are two qualitatively different operating regimes which affect the overall power consumption by the plasma. In a glow discharge, the plasma is uniformly generated across the surface of the reactor. On the contrary in a filamentary discharge, ionization is concentrated in filaments of plasma that appear separated from each other. Figure 5 shows filaments in a plasma, also along the electrode surface. Filamentary discharges consume more electrical power because filaments are self-reinforcing and, as they form, increasing amounts of current flow into the plasma. The ratio of CO_2 volume

Fig. 3 a Minimum discharge voltage peak-to-peak and **b** minimum power as a function of ground electrode temperature in micro DBD reactors with pyramid and flat HV electrodes. Discharge gap: 0.5 mm, CO_2 flow rate: 20 ml min^{-1}, frequency: 68 kHz
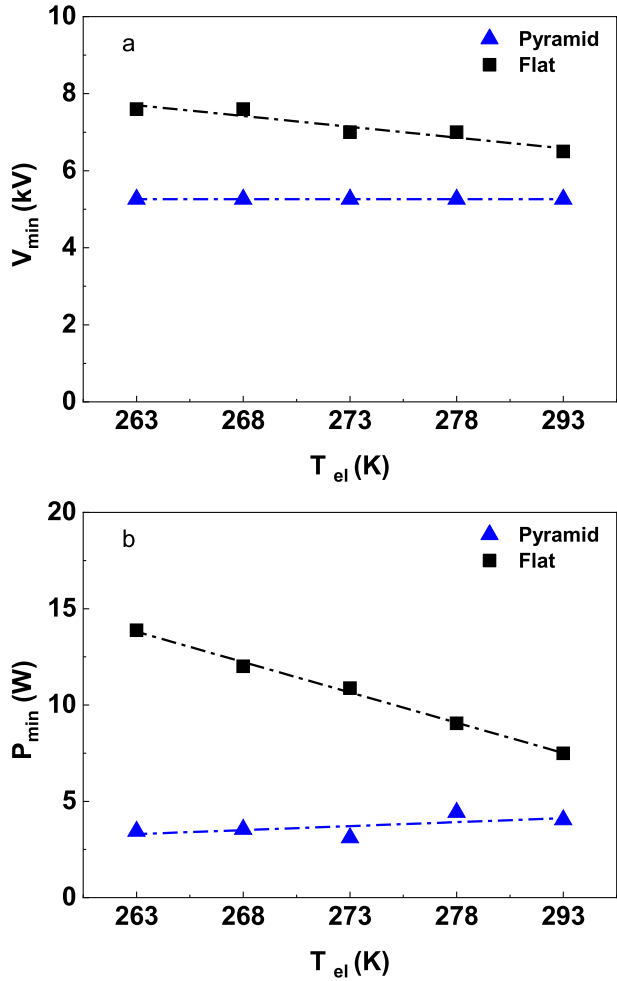

affected by the plasma to the total gas volume in the reactor is lower for filamentary discharges and can affect the overall reaction rate. As a result, the optimization of plasma reactor requires to take all these factors into account.

As the voltage increases to 7 kV, both electrodes have a similar performance and the pyramid electrode has higher rate of energy dissipation at 8.4 kV which is close to the arc formation voltage which results in additional losses.

The CO_2 conversion is shown in Fig. 6 as a function of voltage and discharge power. The conversion increases gradually from 13 to 15% over pyramid electrode and from 9.0 and 10.7% over flat electrode and it always remains by average of 1.5 times higher over pyramid electrode in the entire range studied indicating secondary field emission effect is taking place in pyramid electrode (Fig. 6b). The increase in conversion is small across the applied voltage range for both surfaces, as the variation between 13 to 15 and 9 to 10.7% is small, but across all data points of power and V_{pp}, pyramid electrode shows higher conversion than flat. This serves as evidence to show how electrode surface had significant implications on discharge behaviour in reactor. The pyramid electrode has shown improved

Fig. 4 Lissajous figures at applied voltages of **a** 8.5 kV **b** 7.0 kV, **c** 6.0 kV. Discharge gap: 0.5 mm, CO_2 flow rate: 20 ml min^{-1}
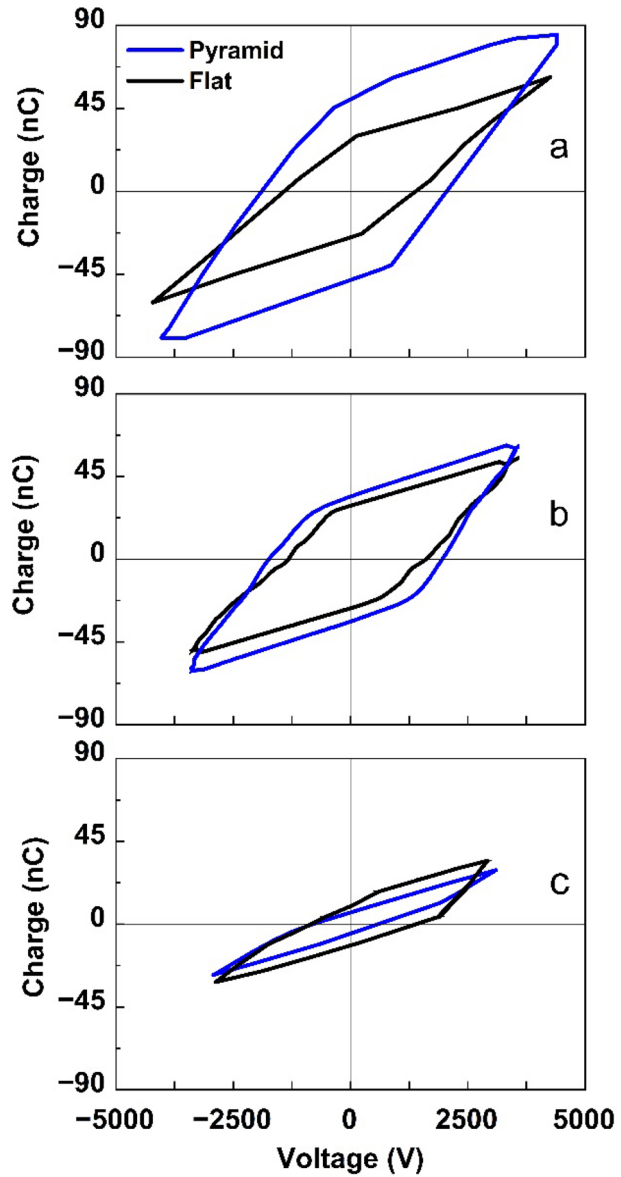
Fig. 5 An optical image of plasma near the pyramid electrode in the pyramid micro DBD reactor to visualize the plasma at a voltage of 6.5 kV. CO_2 flow: 20 ml min^{-1}. The arrows are pointing at the areas near the tips of pyramids where intense light emission can be seen
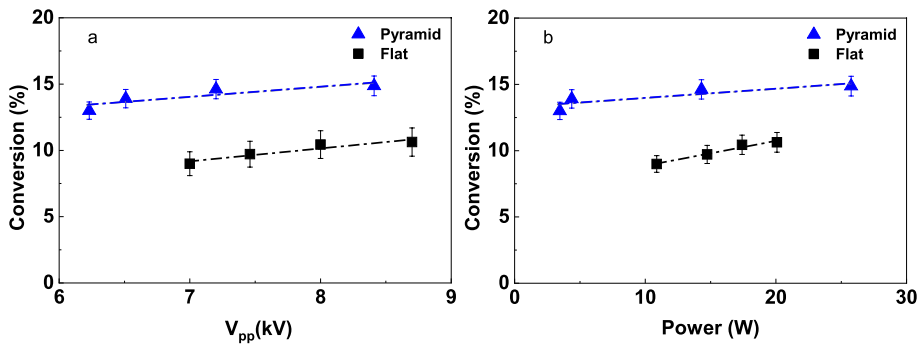
Fig. 6 CO_2 conversion as a function of **a** voltage **b** power for the two electrode configurations. Discharge gap: 0.5 mm, CO_2 flow rate: 20 ml min^{-1}

conversion for lower input power, revealing that surface geometry is an important factor in enhancing DBD reactor performance.

Effect of Discharge Gap Size

The pyramid micro DBD reactor was further studied at two discharge gaps of 0.25 and 0.50 mm. The operation at larger gaps required a higher voltage which resulted in arc formation that could break the mica layer in a longer run. Figure 7 shows current–voltage waveforms at a voltage of 6.5 and 8.0 kV of the AC-driven plasma source. Both electrodes have identical discharge patterns, but the discharges have higher current intensity with the pyramid electrode observed at both voltages. There are multiple current peaks lasting a few nanoseconds in both the rising and declining sections of the voltage.

Production of reactive species such as energetic electrons, ions, and excited atoms depends on the energy per single macrodischarge and coupling of different microdischarges as it influences the temperature and density profile in the reactor [41, 42]. The period when the charge stored on the surface of the dielectric and the number of microdischarges should be increased for a better reactor performance. The current waveforms suggest a filamentous type of discharge pattern in the reactor. The microdischarges are more intense and higher in number at the smaller gap size. The mean time duration of a single discharge increases from 4.6 to 5.2 μs as the gap size decreases. The increase of electric field intensity between the electrodes at the smaller gap size increased the number of microdischarges at both voltages. However, the difference in number of microdischarges reduces at higher voltage.

The corresponding Lissajous figures are shown in Fig. 8. It can be seen that the area increases, and a steeper slope was observed corresponding to an effective capacitance (C_{eff}) of 15 pF at the smaller gap at 6.5 kV. The difference beyween the two gap sizes reduces at a volgate of 8.0 kV, in line with the data on the number of microdischarges. The effective capacitance increases with an increase in discharge power from 15 W (at 0.50 mm) to 22 W (at 0.25 mm) during breakdown, in line with other studies [43].

The total power dissipated in the micro DBD at different voltages is shown in Fig. 9a. The smaller gap increases power consumption, especially at low voltages in the range between 5.0 and 6.3 kV. The slope increases by 1.5 times for the reactor with larger gap size suggesting that power dissipation rate increases faster. The narrow gap allowed the reactor to operate at lower voltage, starting discharge at 5.0 kV, whereas it needs 6.0 kV
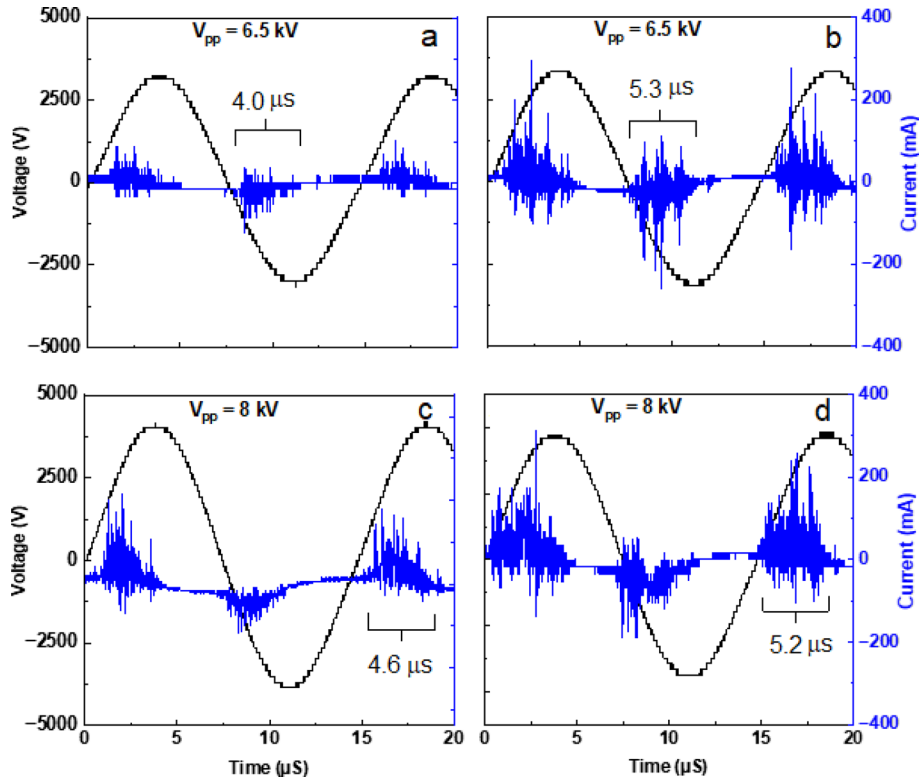
Fig. 7 Typical current–voltage waveforms in the micro DBD reactors with pyramid electrodes. Voltage: 6.5 kV (**a** and **b**), 8.0 kV (**c** and **d**). Gap distance: 0.5 mm (a and c), 0.25 mm (c and d). CO_2 flow: 20 ml min^{-1}
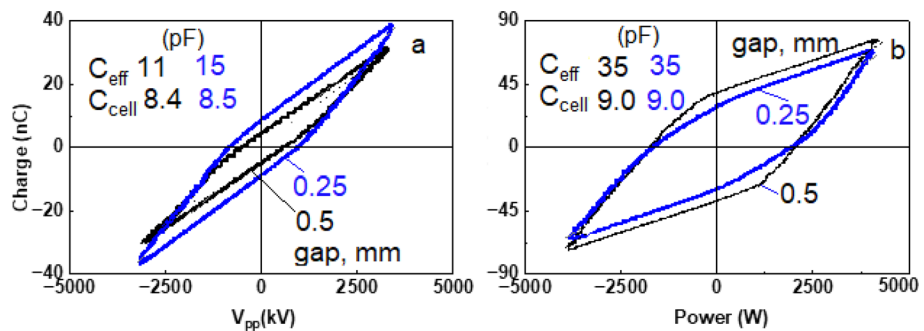
Fig. 8 Lissajous figures in the DBD reactor with the piramid HV electrode. Voltage: **a** 6.5 kV, **b** 8.0 kV. CO_2 flow rate: 20 ml min^{-1}, frequency: 68 kHz

at a gap of 0.5 mm. When the discharge gap increases, the power density of the reactor (discharge power/discharge volume) decreases because the reactive plasma volume
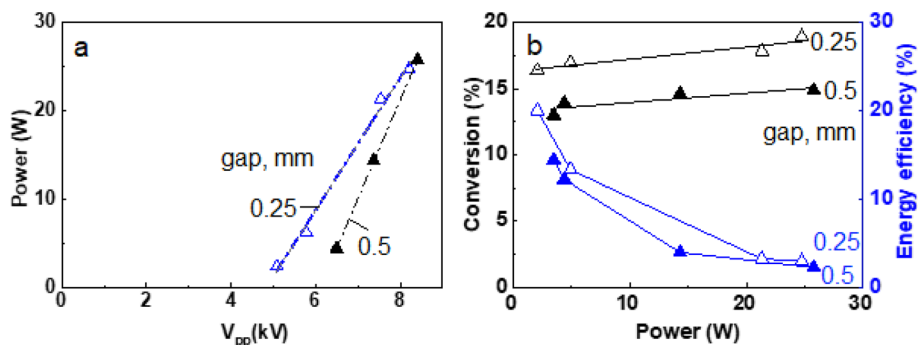
Fig. 9 **a** Power dissipation as a function of voltage, **b** CO_2 conversion and energy efficiency at two discharge gap sizes in the piramid micro DBD reactor. CO_2 flow: 20 ml min^{-1}, frequency 68 kHz

doubles and this results in partial discharging rather than fully bridged discharging, hence less charge formation and lower power consumption [44].

The CO_2 conversion and energy efficiency are shown in Fig. 9b as a function of input power. Increasing discharge gap reduces the maximum CO_2 conversion from 19.0 to 14.9% and the minimum conversion from 16 to 13%. At the same time the highest energy efficiency dropped from 20 to 15%. The improvement in conversion in the reactor with narrow electrode gap was also reported in previous studies [45, 46]. The larger gap size increases the residence time in plasma, however at the same time it decreases the power density which has the dominant influence on the reactor performance. Therefore, the narrow gap improves both conversion and energy efficiency due to increased number of microdischarges and total transferred charge, as discussed above.

As the frequency decreased from 68 to 60 kHz, plasma was made at lower voltages further reducing power consumption. This observation is in line with the data of Ozkan et al. [47]. These authors reported lower CO_2 conversion and lower energy efficiency as the frequency increased from 16.2 to 28.6 kHz, while keeping the same power input. They explained this effect by reduced current amplitude at higher frequency. This effect was also observed in CH_4 conversion in a DBD reactor when conversion dropped by 10% when frequency increased from 20 to 50 kHz at a fixed power of 54 W [48].

It can be seen that operation in the lower power range of about 3 W provides a CO_2 conversion of 16% with an energy efficiency of 20% which may be seen as the optimal operation point for the micro DBD reactor. This combines the advantage of stronger electric fields and higher concentration of electrons, thus combining the advantages of microreactors and microplasma formation. The efficiency in this reactor is on the higher end when compared to the state-of-the-art in DBD reactors.

In our previous study, it was shown that the positive effect of the vibrational ladder climbing process is counteracted by the reduced rate of elementary reaction steps in the temperature range below the electrode temperature of 273 K corresponding to the gas temperature of 363 K [17]. Therefore in the next series of experiments, the temperature of the ground electrode was changed in the 279–293 K range to evaluate its effect on conversion and energy efficiency (Fig. 10). It can be seen that the CO_2 conversion decreases with temperature in the micro DBD reactor as opposed to the case of flat electrode reactor where the conversion increases at lower temperatures. This is the most striking difference between these two reactors. It should be mentioned that while the ground electrode temperature

Fig. 10 CO_2 conversion and energy efficiency as a function of power in the pyramid electrode micro DBD reactor with an electrode gap size of 0.25 mm at three ground electrode temperatures of 279, 283 and 293 K
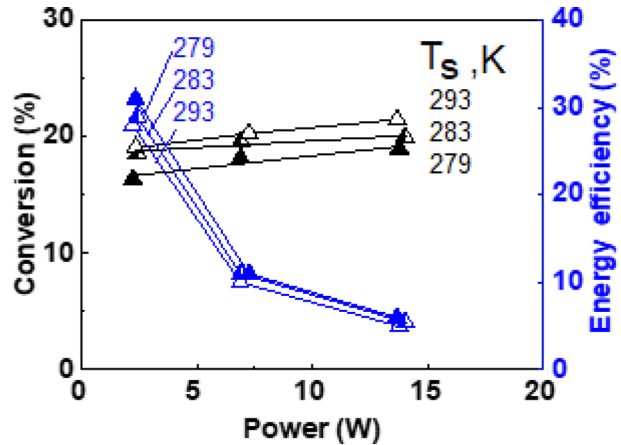
was kept similar in these reactors, the mean gas temperature is significantly different. In the flat electrode reactor, the temperature difference between the gas temperature and the electrode temperature was about 90 K. However, this difference in the pyramid micro DBD reactor seems to be much smaller. The pyramids create natural obstacles to the gas flow and introduce a split-and-recombine flow pattern which enhances heat transfer as compared to laminar flow between the two flat electrodes [49]. In addition, the gap size was reduced in the pyramid reactor by a factor of 2 resulting in a higher superficial CO_2 flow rate, which further increased heat transfer between the plasma and the cold electrode surface. The exact CO_2 gas temperature may be correlated with the temperature of the ground electrode surface following the approach presented in [17]. We can safely assume that the temperature difference between the electrode temperature and the gas temperature can be at least two times smaller due the increased value of heat transfer coefficient in the 0.25 mm gap. In addition, the total amount of power which needs to be removed is less than that in the flat electrode reactor of 15.1 W. Both these facts suggest that the temperature difference between the electrode temperature (T_s) and gas temperature (T) should not exceed 40 K at the highest power (Q) in the pyramid reactor, assuming that 95% of power dissipates as heat (Fig. 9).

$$Q = hA(T - T_s), \tag{5}$$

where A is the area of the electrode, $2.99 \cdot 10^{-4}$ m^2. In our previous studies, we recognized the need to characterize the temperature of the gas and therefore a detailed measurement of CO_2 rotational temperature in the micro DBD reactor was performed and correlated with the gas temperature [17, 50]. It was concluded that Eq. 5 makes a rather good prediction which is in line with the experimental data obtained by optical emission spectroscopy (OES) analysis. Measuring temperature with OES was outside the scope of this work, yet based on the results obtained in [17] we may conclude that the maximum gas temperature should not exceed 333 K at the electrode temperature of 293 K. This value is below the optimum gas temperature of 363 K observed in [17] and therefore the conversion increases with temperature in the whole temperature range (Fig. 10), because chemical reaction rates increase with temperature. The sensitivity of CO_2 plasma chemistry to the gas temperature shows the need for a better understanding of the temperature behaviour. The relevant gas temperatures are in the range between 343 and 383 K, which were not studied in this

reactor due to its technical limitations. We anticipate higher electrode and gas temperature may further improve CO_2 conversion however at the expense of energy efficiency. Similar to the case of flat electrode, the conversion further increases with input power while the energy efficiency drops by more than 3 times at the same time. These estimations help to understand the process conditions and guide further process development.

Effect of Residence Time

The pyramid micro DBD reactor was studied a constant gas flow rate of 20 ml min^{-1} corresponding to a nominal residence time of 1.0 s in all experiments thus far, and the last series of experiments was carried out to study the effect of CO_2 flow rate at two voltages of 6.5 and 8.0 kV as the contact time in plasma has a major influence on the reaction rate. In the absence of mass transfer limitations in a conventional flow reactor, the reaction rate does not depend on the reactant flow rate. However, in a plasma reactor, the spatial distribution of plasma density may be non-uniform across the discharge volume. Also, it is well known that due to the presence of charged particles, plasma has a higher viscosity than the respective gas at the same temperature and pressure. Therefore, there may exist preferred flow pathways between different sets of pyramids and the reactor behaviour may be non-ideal. The area with higher density would create a higher hydrodynamic resistance to the flow therefore the flow rate in such areas would be lower [51]. Therefore the contribution from such areas to the overall conversion of CO_2 may be very low.

A possible way to improve the situation is to increase the gas flow rate in the reactor which usually results in a more uniform distribution of the flow as the overall hydrodynamic resistance increases and any local differences between various pathways become less significant. Indeed, several researchers noted that a much higher efficiency was obtained at higher CO_2 flow rates, with energy efficiency increasing from 3.6% at a flow rate of 20 ml min^{-1} to 7.0% at a flow rate of 60 ml min^{-1} [52]. In the following experiments, the flow rate was increased from 10 to 80 ml min^{-1} resulting in residence time in the range between 2.0 and 0.25 s. The respective Lissajous figures are shown in Figs. 11a and b. The power consumption reduces at higher flow rates (60 and 80 ml min^{-1} Fig. 11c) resulting in increase in energy efficiency at higher flow rates corresponding to shorter residence times (Fig. 11c). The maximum CO_2 conversion of 20.3% was observed at the longest residence time and it is decreases to 3.9% at shorter residence time (Fig. 11d). It is important to note that the reaction rate changes with flow rate which a clear evidence of mass transfer limitations and/or the presence of stagnant zones in the reactor. For example, increasing the flow rate from 20 to 40 ml min^{-1} results in increasing reaction rate from om 2.28 to 2.80 μmol CO_2 s^{-1}. However, further increase in flow rate from 40 to 80 mL min^{-1} reduces the reaction rate to 2.32 μmol CO_2 s^{-1}. It is possible that higher flow rate results in a more uniform spatial distribution of the reactant and eliminates stagnant zones that can be present at very low flow rates.

Nacascues et al. [23] reported that CO_2 conversion increased at higher flow rates in a packed bed DBD reactor, unlike the findings of other authors [10, 11] tentatively attributing this to potential backwards reactions taking place on the surface or in the plasma bulk (e.g. $CO + O \rightarrow CO_2$). However it is more likely that high viscosity of plasma as compared to non-ionised gas creates preferred pathways for the fluid flow. In the plasma, if the mean velocity of a certain plasma component is space inhomogeneous, there are the momentum currents to move from a high velocity layer to a low velocity areas. As a result, more gas passing through the area with low viscosity corresponding to low intensity plasma, while
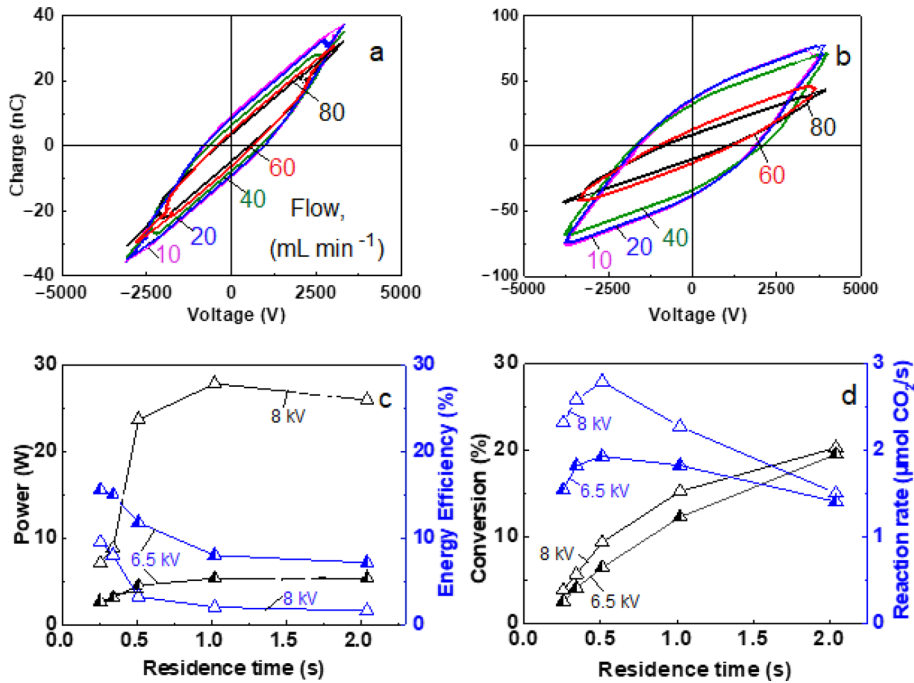
Fig. 11 Lissajous figures in the pyramid micro DBD reactror. Voltage: **a** 6.5 kV, **b** 8.0 kV. **c** Energy efficiency and power consumtion as a functrion of residence time at the two selected voltages, **d** CO_2 conversion and reaction rate as a functrion of residence time at the two selected voltages. Frequency: 68 kHz

less gas goes via the areas with strong ionisation. However, as the flow rate increases, the overall pressure drop across the reactor increases and the differences between individual parts of the reactor becomes less significant. Therefore the fraction of the gas passing through the area of more intense plasma increases. Also as the flow rate increases, the weakly ionized plasma contains less charged particle than neutral particle. The interactions between particles are taking place by the collisions, such as electron–electron collision, electron–ion collision, electron-neutral-particle collision and ion-neutral-particle collision. Since the number of charged particles is smaller at higher flow rate, the viscosity is mainly determined by collisions of charged particles with the neutral particles and the collisions between the charged particles can be neglected so the viscosity of plasma becomes more uniform.

This effect may be responsible for an increase in the reaction rate at higher flow rates. Naturally, the probability of the backward recombination reaction also decreases, however its characteristic time is in the order of microseconds which is too short as compared to the residence time which is in the second range. Therefore, we may assume that hydrodynamics and momentum transfer effects are responsible for such behavior rather than reaction kinetics.

However as the residence time decreases, the reaction rate starts to decline. This is somehow expected as the density of charged particles decreases with power density resulting in a decrease in CO_2 conversion. Therefore, there exists an optimal flow rate of 40 ml min^{-1} where the counterplay between these two effects produces the best result. It

should be noted that a rather small increase in voltage from 6.5 to 8.0 kV increases the power dissipation from 5.4 to 25.6 W, however this has a very little effect on CO_2 conversion. In fact, the conversion increases marginally from 19.0 to 20.3%. This supports the previous assumption on a very non-uniform gas distribution along the reactor cross-section at low flow rate. Increasing the power does not improve conversion at low flow rates as the gas does not pass via highly ionised areas. On the contrary, at a higher flow rate of 80 ml min^{-1} a power increase from 2.7 to 7.1 W increases CO_2 conversion from 2.6 to 4.0% as more gas passes via strongly ionised plasma areas. This is in line with other studies where a positive effect of increasing flow rate was observed in DBD reactors [53, 54]. The flow rate has clearly a major influence on CO_2 conversion in the pyramid reactor and for highly efficient operation, the gas recycling loop is needed to increase overall conversion and make it feasible for subsequent product separation.

Conclusions

A novel plate to plate micro DBD reactor with pyramid shaped microelectrodes was designed and tested for CO_2 splitting into CO and O_2. The performance was compared with a conventional plate-to-plate reactor with two flat electrodes which was considered as a benchmark. The pyramid micro DBD reactor consistently outperformed the baseline case by about 1.5 times at the same process parameters. The big difference with the base case was observed at a smaller discharge gap, allowing reactor to operate at lower voltage, which further improved CO_2 conversion and increasing energy efficiency by 1.25 times. The pyramid micro DBD reactor created a local flow disturbance which drastically increased heat transfer between the cold electrode and the surrounding gas. As a result, the temperature difference between the gas and the electrode surface is limited to 40 K as compared to 90 K for the baseline case. The cold gas effectively suppresses the vibrational to translational energy transfer which dominates in the reactor with flat electrode. As the flow rate increases, the fraction of the gas passing through the area of more intense plasma increases while at the same time the density of charged particles decreases. The interplay between these two effects results in an optimum residence time of 0.5 s which provides the maximum CO_2 reaction rate.

Thus it has been shown that the size of the gap in which plasma forms, the distance along the length in the flow direction (residence time) and the geometric shape of the electrodes could considerably enhance the rate of CO_2 splitting reaction in the micro DBD reactor. It has been demonstrated that each of these factors will yield substantial improvements to either or both reactor yield and energy efficiency, thus enabling energy efficient process which provides a CO_2 conversion of 20% with an energy efficiency of 16% in a micro DBD reactor. The best energy consumption numbers are competitive with the state of the art for DBD based NTP systems. Further enhancement is anticipated by application of thin catalyst layers onto the ground electrode and the way the waveforms are produced in the reactor. The electric field, and ionization of CO_2, is the highest where the slope of the AC sinusoid is steepest but is ultimately limited by the requirement of a smooth shape of sinusoidal waveform. An alternate approach is to apply pulsed direct current (pulsed DC) waveforms where the fall and rise times from positive to negative high voltage can be in the order of tens of nanoseconds compared to microseconds for AC, a difference of 10–50 times. The more rapidly changing electric field for pulsed DC mode may produce higher rates of ionization.

Authors' Contributions D.K. performed all experiments, wrote the main manuscript text and prepared all figures with support from S.L. and E.R. A.C., S.L., N.C. conceived and planned the experiments. E.R supervised the project. All authors reviewed the manuscript.

Data Availability Data will be made available on request.

Declarations

Conflict of interests We declare that the authors have no conflict of interests as defined by Springer, or other interests that might be perceived to influence the results and/or discussion reported in this paper.

Ethical approval N/A.

References

1. Li S, Liu C, Bogaerts A, Gallucci F (2022) Editorial: Special issue on CO_2 utilization with plasma technology. J CO2 Util 61:102017. https://doi.org/10.1016/j.jcou.2022.102017
2. de la Fuente JF, Moreno SH, Stankiewicz AI, Stefanidis GD (2016) A new methodology for the reduction of vibrational kinetics in non-equilibrium microwave plasma: application to CO_2 dissociation. React Chem Eng 1:540–554. https://doi.org/10.1039/C6RE00044D
3. Hotta SK, Sahoo N, Mohanty K (2019) Ignition advancement study for optimized characteristics of a raw biogas operated spark ignition engine. Int J Green Energy 16:101–113. https://doi.org/10.1080/15435075.2018.1544901
4. Abanades S (2022) Redox cycles, active materials, and reactors applied to water and carbon dioxide splitting for solar thermochemical fuel production: a review. Energies 15:7061. https://doi.org/10.3390/en15197061
5. Liu J-L, Wang X, Li X-S, et al (2020) CO 2 conversion, utilisation and valorisation in gliding arc plasma reactors. J Phys D Appl Phys 53:253001. https://doi.org/10.1088/1361-6463/ab7c04
6. Snoeckx R, Bogaerts A (2017) Plasma technology – a novel solution for CO_2 conversion? Chem Soc Rev 46:5805–5863. https://doi.org/10.1039/C6CS00066E
7. Tran NN, Tejada JO, Asrami MR et al (2021) Economic optimization of local australian ammonia production using plasma technologies with green/turquoise hydrogen. ACS Sustain Chem Eng 9:16304–16315. https://doi.org/10.1021/acssuschemeng.1c05570
8. Rackley S (2017) Carbon capture and storage, 2nd edn. Elsevier
9. Van Laer K, Bogaerts A (2015) Improving the conversion and energy efficiency of carbon dioxide splitting in a zirconia-packed dielectric barrier discharge reactor. Energy Technol 3:1038–1044. https://doi.org/10.1002/ente.201500127
10. Uytdenhouwen Y, Van Alphen S, Michielsen I et al (2018) A packed-bed DBD micro plasma reactor for CO_2 dissociation: does size matter? Chem Eng J 348:557–568. https://doi.org/10.1016/j.cej.2018.04.210

11. Abiev RS, Sladkovskiy DA, Semikin KV et al (2020) Non-thermal plasma for process and energy intensification in dry reforming of methane. Catalysts 10:1358. https://doi.org/10.3390/catal10111358

12. Dębek R, Azzolina-Jury F, Travert A, Maugé F (2019) A review on plasma-catalytic methanation of carbon dioxide – Looking for an efficient catalyst. Renew Sustain Energy Rev 116:109427. https://doi.org/10.1016/j.rser.2019.109427

13. Chen H, Mu Y, Xu S et al (2020) Recent advances in non-thermal plasma (NTP) catalysis towards C1 chemistry. Chinese J Chem Eng 28:2010–2021. https://doi.org/10.1016/j.cjche.2020.05.027

14. Li S, Rebrov E, Gallucci F, Hessel V (2022) CO_2 hydrogenation with a dielectric barrier discharge reactor. In: Chemical valorisation of carbon dioxide. The Royal Society of Chemistry, pp 446–465

15. Mei D, Tu X (2017) Atmospheric pressure non-thermal plasma activation of CO_2 in a packed-bed dielectric barrier discharge reactor. ChemPhysChem 18:3253–3259. https://doi.org/10.1002/cphc.201700752

16. Bogaerts A, Centi G, Hessel V, Rebrov E (2023) Challenges in unconventional catalysis. Catal Today 420:114180. https://doi.org/10.1016/j.cattod.2023.114180

17. Khunda D, Li S, Cherkasov N et al (2023) Effect of temperature on the CO_2 splitting rate in a DBD microreactor. React Chem Eng. https://doi.org/10.1039/D3RE00113J

18. Mei D, Sun M, Liu S et al (2023) Plasma-enabled catalytic dry reforming of CH_4 into syngas, hydrocarbons and oxygenates: Insight into the active metals of γ-Al_2O_3 supported catalysts. J CO2 Util 67:102307. https://doi.org/10.1016/j.jcou.2022.102307

19. Li D, Rohani V, Fabry F et al (2020) Direct conversion of CO_2 and CH_4 into liquid chemicals by plasma-catalysis. Appl Catal B Environ 261:118228. https://doi.org/10.1016/j.apcatb.2019.118228

20. Biset-Peiró M, Guilera J, Zhang T et al (2019) On the role of ceria in Ni-Al_2O_3 catalyst for CO_2 plasma methanation. Appl Catal A Gen 575:223–229. https://doi.org/10.1016/j.apcata.2019.02.028

21. Van Laer K, Bogaerts A (2017) How bead size and dielectric constant affect the plasma behaviour in a packed bed plasma reactor: a modelling study. Plasma Sources Sci Technol 26:085007. https://doi.org/10.1088/1361-6595/aa7c59

22. Zhu M, Hu S, Wu F et al (2022) CO_2 dissociation in a packed bed DBD reactor: effect of streamer discharge. J Phys D Appl Phys 55:225207. https://doi.org/10.1088/1361-6463/ac55c1

23. Zhang K, Zhang G, Liu X et al (2017) A study on CO_2 decomposition to CO and O_2 by the combination of catalysis and dielectric-barrier discharges at low temperatures and ambient pressure. Ind Eng Chem Res 56:3204–3216. https://doi.org/10.1021/acs.iecr.6b04570

24. Navascués P, Cotrino J, González-Elipe AR, Gómez-Ramírez A (2022) Plasma assisted CO_2 dissociation in pure and gas mixture streams with a ferroelectric packed-bed reactor in ambient conditions. Chem Eng J 430:133066. https://doi.org/10.1016/j.cej.2021.133066

25. Renninger S, Stein J, Lambarth M, Birke KP (2022) An optimized reactor for CO_2 splitting in DC atmospheric pressure discharge. J CO2 Util 58:101919. https://doi.org/10.1016/j.jcou.2022.101919

26. Lee JH, Kim YS, Kyung SJ et al (2009) Characteristics of SiOx thin films deposited by using direct-type pin-to-plate dielectric barrier discharge with PDMS/He/O2 gases at low temperature. J Korean Phys Soc 54:981–985. https://doi.org/10.3938/jkps.54.981

27. Jidenko N, Petit M, Borra JP (2006) Electrical characterization of microdischarges produced by dielectric barrier discharge in dry air at atmospheric pressure. J Phys D Appl Phys 39:281–293. https://doi.org/10.1088/0022-3727/39/2/008

28. Peeters FJJ, Yang R, van de Sanden MCM (2015) The relation between the production efficiency of nitrogen atoms and the electrical characteristics of a dielectric barrier discharge. Plasma Sources Sci Technol 24:045006. https://doi.org/10.1088/0963-0252/24/4/045006

29. Pourali N, Sarafraz MM, Hessel V, Rebrov EV (2021) Simulation study of a pulsed DBD with an electrode containing charge injector parts. Phys Plasmas 28:013502. https://doi.org/10.1063/5.0027562

30. Pourali N, Hessel V, Rebrov EV (2022) The effects of pulse shape on the selectivity and production rate in non-oxidative coupling of methane by a Micro-DBD reactor. Plasma Chem Plasma Process 42:619–640. https://doi.org/10.1007/s11090-022-10242-6

31. Takaki K, Shimizu M, Mukaigawa S, Fujiwara T (2004) Effect of electrode shape in dielectric barrier discharge plasma reactor for NOx removal. IEEE Trans Plasma Sci 32:32–38. https://doi.org/10.1109/TPS.2004.823973

32. Takaki K, Shimizu M, Sasaki T, et al (2003) Flue gas treatment using dielectric barrier discharge with multipoint electrode. In: Digest of Technical Papers. PPC-2003. 14th IEEE international pulsed power conference (IEEE Cat. No.03CH37472). IEEE, pp 571–574

33. Liu P, Chen B, Liang C et al (2021) Tip-enhanced electric field: a new mechanism promoting mass transfer in oxygen evolution reactions. Adv Mater 33:2007377. https://doi.org/10.1002/adma.202007377

34. Banerjee AM, Billinger J, Nordheden KJ, Peeters FJJ (2018) Conversion of CO_2 in a packed-bed dielectric barrier discharge reactor. J Vac Sci Technol A 36:04F403. https://doi.org/10.1116/1.5024400

35. Pipa AV, Koskulics J, Brandenburg R, Hoder T (2012) The simplest equivalent circuit of a pulsed dielectric barrier discharge and the determination of the gas gap charge transfer. Rev Sci Instrum 83:115112. https://doi.org/10.1063/1.4767637

36. Wang S, Zhang Y, Liu X, Wang X (2012) Enhancement of CO_2 conversion rate and conversion efficiency by homogeneous discharges. Plasma Chem Plasma Process 32:979–989. https://doi.org/10.1007/s11090-012-9386-8

37. Zhu S, Zhou A, Yu F et al (2019) Enhanced CO_2 decomposition via metallic foamed electrode packed in self-cooling DBD plasma device. Plasma Sci Technol 21:085504. https://doi.org/10.1088/2058-6272/ab15e5

38. Pinhão N, Moura A, Branco JB, Neves J (2016) Influence of gas expansion on process parameters in non-thermal plasma plug-flow reactors: a study applied to dry reforming of methane. Int J Hydrogen Energy 41:9245–9255. https://doi.org/10.1016/j.ijhydene.2016.04.148

39. Dunbar WG, Seabrook JW (1976) High voltage design guide for airborne equipment. Boeing Aerospace CO Seattle WA

40. Li S-Z, Uhm HS (2004) Investigation of electrical breakdown characteristics in the electrodes of cylindrical geometry. Phys Plasmas 11:3088–3095. https://doi.org/10.1063/1.1736656

41. Uhm HS, Jung SJ, Kim HS (2003) Influence of gas temperature on electrical breakdown in cylindrical electrodes. J Korean Phys Soc 42:989–993

42. Jidenko N, Bourgeois E, Borra J-P (2010) Temperature profiles in filamentary dielectric barrier discharges at atmospheric pressure. J Phys D Appl Phys 43:295203. https://doi.org/10.1088/0022-3727/43/29/295203

43. Tschiersch R, Nemschokmichal S, Bogaczyk M, Meichsner J (2017) Surface charge measurements on different dielectrics in diffuse and filamentary barrier discharges. J Phys D Appl Phys 50:105207. https://doi.org/10.1088/1361-6463/aa5605

44. Mei D, Tu X (2017) Conversion of CO_2 in a cylindrical dielectric barrier discharge reactor: effects of plasma processing parameters and reactor design. J CO2 Util 19:68–78. https://doi.org/10.1016/j.jcou.2017.02.015

45. Aerts R, Somers W, Bogaerts A (2015) Carbon dioxide splitting in a dielectric barrier discharge plasma: a combined experimental and computational study. Chemsuschem 8:702–716. https://doi.org/10.1002/cssc.201402818

46. Kamkeng ADN, Wang M, Hu J et al (2021) Transformation technologies for CO_2 utilisation: current status, challenges and future prospects. Chem Eng J 409:128138. https://doi.org/10.1016/j.cej.2020.128138

47. Ozkan A, Dufour T, Silva T et al (2016) The influence of power and frequency on the filamentary behavior of a flowing DBD—application to the splitting of CO_2. Plasma Sources Sci Technol 25:025013. https://doi.org/10.1088/0963-0252/25/2/025013

48. Liu SY, Mei DH, Shen Z, Tu X (2014) Nonoxidative conversion of methane in a dielectric barrier discharge reactor: prediction of reaction performance based on neural network model. J Phys Chem C 118:10686–10693. https://doi.org/10.1021/jp502557s

49. Wang Q, Hessel V, Rebrov EV, Werner B (2011) 3D analysis of heat transfer intensification by re-entrance flow pin-fins microstructures with a highly thermal-conductive plate. Chem Eng Technol 34:379–390. https://doi.org/10.1002/ceat.201000376

50. Pourali N, Lai K, Gregory J et al (2023) Study of plasma parameters and gas heating in the voltage range of nondischarge to full-discharge in a methane-fed dielectric barrier discharge. Plasma Process Polym 20:2200086. https://doi.org/10.1002/ppap.202200086

51. Rebrov EV, Schouten JC, de Croon MHJM (2011) Single-phase fluid flow distribution and heat transfer in microstructured reactors. Chem Eng Sci 66:1374–1393. https://doi.org/10.1016/j.ces.2010.05.044

52. Wang J-Y, Xia G-G, Huang A et al (1999) CO_2 decomposition using glow discharge plasmas. J Catal 185:152–159. https://doi.org/10.1006/jcat.1999.2499

53. Afriansyah R, Nadhifa S, Bismo S (2018) Performance test and operating condition optimization of parallel plate plasma reactor for carbon dioxide decomposition. Int J Technol 9:1151. https://doi.org/10.14716/ijtech.v9i6.2363

54. Gómez-Ramírez A, Montoro-Damas AM, Rodríguez MA et al (2017) Improving the pollutant removal efficiency of packed-bed plasma reactors incorporating ferroelectric components. Chem Eng J 314:311–319. https://doi.org/10.1016/j.cej.2016.11.065